

ChemComm

Accepted Manuscript



This is an *Accepted Manuscript*, which has been through the Royal Society of Chemistry peer review process and has been accepted for publication.

Accepted Manuscripts are published online shortly after acceptance, before technical editing, formatting and proof reading. Using this free service, authors can make their results available to the community, in citable form, before we publish the edited article. We will replace this *Accepted Manuscript* with the edited and formatted *Advance Article* as soon as it is available.

You can find more information about *Accepted Manuscripts* in the [Information for Authors](#).

Please note that technical editing may introduce minor changes to the text and/or graphics, which may alter content. The journal's standard [Terms & Conditions](#) and the [Ethical guidelines](#) still apply. In no event shall the Royal Society of Chemistry be held responsible for any errors or omissions in this *Accepted Manuscript* or any consequences arising from the use of any information it contains.



Journal Name

ARTICLE

Recent Advances in the Application of Total Scattering Methods to Function Materials

Received 00th January 20xx,
Accepted 00th January 20xx

DOI: 10.1039/x0xx00000x

www.rsc.org/

Alessandro Mancini,^a Lorenzo Malavasi^{a,*}

In this Feature Article we provide a description of some of the most recent results obtained in the field of materials science by means of total scattering methods and PDF analysis. Particular attention is devoted to the application of PDF to functional materials and to examples showing the combination of PDF with other solid state chemistry techniques.

1. Introduction

Understanding the correlation between structural and mechanistic properties represents the core problem of modern materials chemistry. Fundamental advances in this research field have been made thanks to countless crystallographic studies in the past decades and have been allowed by the continuous development of the structural analysis carried out by traditional methods, *i.e.* X-ray and neutron diffraction. In more recent times, however, there is a growing realization of the limits provided by the traditional crystallographic approaches, which are based on the assumption of lattice periodicity. In fact, the appearance of new functional materials, increasingly more advanced and complex, such as, for example, nanocrystalline compounds or highly defective oxides, clearly showed how diffraction alone cannot provide a careful description of materials structures. In these new materials, the correlation between physical properties and structural, electronic or magnetic inhomogeneity has become evident, with their functional properties strongly connected to the deviations from the average structure. For this reason, new experimental approaches, which are able to take into account local structure details, gained growing importance in the crystallographic investigation¹⁻³.

Traditionally, the local structure analysis of crystalline materials has been afforded by means of EXAFS and solid state NMR, which have different targets and sensitivities in comparison with crystallography methods. The dominant contribution to these probes is given by the structural correlations between nearest neighbours; thus they can provide very useful information on the coordination environment with respect to a reference atom but, on the other hand, they basically do not provide any information coming from longer distances. As a matter of fact, this difference in target information sometimes generates structural results which seem apparently in contradiction between EXAFS/NMR and

crystallography¹. In this context, it is evident the need of a probe which can be able to act as a bridge between the two domains of the average and the local structure, *i.e.* that can provide an effective description of the structure of a material on different length scales, both considering the long range order and the possible deviation from it at the local level. In order to meet this need, new experimental approaches have been developed in recent times. In particular, the total scattering methods coupled to the Pair Distribution Function analysis (PDF) has gained progressively a central role in the understanding of the structure-properties correlation starting from its extensive application to solid state problems in the late '90s⁴. This is witnessed by the number of materials chemistry works which take advantage of this technique and by the number of dedicated instruments present, or planned to be built, in international facilities.

In this Feature Article, after a concise description of the PDF technique, we are going to summarize the more recent advances in the application of total scattering methods to the investigation of crystalline and nanocrystalline functional materials. Attention will be also paid on recent experiments carried out in *in situ* or *in operando* conditions in order to show the great applicative potential of these methods. Similarly, works carried out by coupling PDF analysis with other experimental or theoretical techniques will be discussed to emphasize how a multi-technique approach can be a powerful tool to afford challenging problems in materials chemistry. Great prominence will also be given to the wide range of different application fields where PDF provided significant contributions in recent times, showing how this technique is powerful in providing information at the atomic scale level.

2. Atomic pair distribution function technique

In this section we provide the basic mathematical and physical information regarding the PDF technique. However, we invite the reader to refer to Ref. 4 for a more detailed discussion. As can be

^a Department of Chemistry and INSTM, Viale Taramelli 16, 27100 Pavia, Italy
Corresponding Author: Lorenzo.malavasi@unipv.it

guessed, the *total scattering* approach uses both the Bragg and diffuse scattering on an equal basis. The analysis of the Bragg peaks provide information about the average structure of the investigated material, such as cell parameters, atomic positions and thermal displacements, while the diffuse scattering account for static or dynamical disorder, *i.e.* for local deviations from the long range order. From an experimental point of view, the data are measured as in a regular powder diffraction experiment. The experimental intensity measured, $I(Q)$, is expressed as:

$$I(Q) = PA[N(I^{coh} + I^{inc} + I^{mul})] \quad (1)$$

where P is the polarization factor, A is the absorption coefficient, N is a normalization constant to the incident flux and I^{coh} , I^{inc} , and I^{mul} , are the coherent, incoherent and multiple scattering intensities, respectively. In addition, also the background intensity arising from effects as the scattering from air and sample environment has to be considered (*i.e.* measured and then subtracted from the total experimental intensity measured, $I(Q)$). Let us note that $I(Q)$ is a continuous function of Q , the magnitude of the scattering vector, which is defined as:

$$Q = \frac{4\pi \sin \theta}{\lambda} \quad (2)$$

where θ is half of the scattering angle. The *total scattering structure function*, $S(Q)$, is obtained by dividing $I(Q)$ by the numbers of scatterers so that $S(Q)$ is in absolute units of scattering-per-atom⁴. In the case of an X-ray experiment it can be defined as:

$$S(Q) = \frac{I^{coh} - \langle f^2 \rangle + \langle f \rangle^2}{\langle f \rangle^2} \quad (3)$$

where $\langle f \rangle^2$ and $\langle f^2 \rangle$ are the square of the mean and the mean square scattering factors of the sample respectively. In the case of neutron experiments, the Q -independent neutron scattering lengths (b) are used. In order to obtain the $S(Q)$ function, $I(Q)$ data have to be suitably corrected before for absorption, polarization factor, multiple scattering, incoherent scattering, background, and they have to be properly normalized^[5-7]. $S(Q)$ is a dimensionless quantity and, due to the normalization used, its average value is 1, *i.e.* $\langle S(Q) \rangle = 1$. This average is performed over the Q -range probed. It should be stressed that the total scattering factor is nothing other than the powder diffraction pattern that has been corrected for experimental artefacts and suitably normalized. In the PDF analysis we are interested in obtaining what is called the *reduced pair distribution function*, $G(r)$, which is defined as:

$$G(r) = 4\pi r[\rho(r) - \rho_0] \quad (4)$$

where $\rho(r)$ is the microscopic pair density and ρ_0 is the average number density. The direct Fourier transform of the $S(Q)$ function generates the experimental $G(r)$ ^[8]:

$$G(r) = \frac{2}{\pi} \int_0^\infty Q[S(Q) - 1] \sin(Qr) dQ \quad (5)$$

The $G(r)$ can be calculated from a structural model using:

$$G_c(r) = \frac{1}{r} \sum_i \sum_j \left[\frac{f_i(0)b_j}{\langle b \rangle^2} \delta(r - r_{ij}) \right] - 4\pi\rho_0 \quad (6)$$

where f_v and f_μ and are the scattering factors for atoms v and μ and $\langle f \rangle^2$ has the same meaning as in eq. (3). The sum is performed over all pairs of atoms v and μ separated by $r_{v\mu}$. Again, in the case of a neutron experiment the f are replaced by Q -independent neutron scattering lengths (b). $G(r)$ oscillates around 0 and, in the case of an X-ray experiment, a peak in the $G(r)$ pattern indicates a r -range where the probability of finding inter-atomic vectors is greater than that determined by the number density ($\rho(r) > \rho_0$); conversely, the same probability is lower ($\rho_0 > \rho(r)$) in correspondence of a negative peaks in the $G(r)$. $G(r)$ reduces to $-4\pi\rho_0 r$ when $r \rightarrow 0$, due to the lack of physical inter-atomic distances, while $G(r) \rightarrow 0$ when $r \rightarrow \infty$ ⁴. One important "practical" aspect of collecting PDF data relates to the Q -range probed. As can be appreciated from eq. 5 the $S(Q)$ is measured only over a finite range of Q . In practice, the real-space resolution of the PDF is directly related to the range of Q over which data are measured; roughly speaking $\delta r = \pi/Q_{\max}$ where Q_{\max} is the maximum Q -value⁴. As a matter of fact, in order to increase the Q_{\max} it is necessary to decrease the λ used in the experiment according to eq. 2. This can be obtained by using spallation neutron sources with a high flux of epithermal neutrons with short wavelengths or by collecting X-ray diffraction data at high-energy synchrotron facilities using short wavelengths. For X-rays experiments there is the additional challenge related to the drop-off of the X-ray form factor with Q , resulting in a weak signal at high diffracting angles. However, suitable high-energy synchrotrons allow to get sufficient statistics to yield accurate data up to at least 45 \AA^{-1} . The importance of collecting the data to high Q_{\max} values is also related to the spurious oscillations, called "termination ripples", that are present due to the finite Q range of the experiment (ripples with a wavelength $\sim 2\pi/Q_{\max}$)^[4]. However, the coherent intensity (features) in the $S(Q)$ dies out with increasing Q due to the Debye-Waller factor so that suitable PDFs are obtained by terminating the data at $Q_{\max} \sim 3/\langle \langle u^2 \rangle \rangle^{1/2}$, where $\langle \langle u^2 \rangle \rangle^{1/2}$ is the root mean square of lattice vibrations^[9]. Overall, by a Q -value of 30-50 \AA^{-1} (depending on temperature and stiffness of the bonding) there are no more features in the $S(Q)$ and there is no need to measure to higher- Q . As briefly mentioned above, the PDF reflects both the long-range atomic structure, manifest in the sharp Bragg peaks, and the local structural imperfections, manifest in the diffuse components of the diffraction pattern. This is because the *total scattering* contributes to the PDF. The analysis of the data does not presume periodicity. Some information can be directly extracted from the PDF because of its definition as the atom-pair correlation function⁴. For example, from the peak-position it is possible to

extract information about the bond length because the presence of a peak in the PDF indicates the existence of a pair of atoms with that separation. The peak integrated intensities instead give information about the coordination number because it is influenced by the number of neighbours in that coordination shell around an origin atom. Finally, the measurement of the peak width may allow to extract information about the thermal or static disorder since it gives rise to a distribution of atom-atom distances¹⁰.

Modelling the data, however, reveals much more information than the only model-independent analysis. The most popular approach is the real-space modelling with the use of a full-profile fitting method analogous to the Rietveld method but where the function fitted is the PDF. This is implemented in the PDFgui program¹¹ which is the most recent version of the PDFfit software¹². In this method, parameters of the structural calculated model (lattice constants, atomic position and atomic displacement parameters) and other experiment-dependent parameters are allowed to vary with a least-square approach until they reach the best-fit with respect to the experimental functions. In comparison with a Rietveld refinement, however, it is possible to model the short range $G(r)$ by using unit cells with different sizes (*i.e.*, supercells), reduce the symmetry of the structure and introduce disorder. In other words, it is possible to model the function without any periodicity assumption. For a more detailed treatment of this topic we suggest the reader to Ref 4. PDF can be also modelled in the reciprocal space with methods that generally involve larger models of thousands of atoms that are usually refined using Monte Carlo simulated annealing or some other global optimization scheme. A quite popular approach is the reverse Monte Carlo (RMC) where the quantity to be minimized is the difference between a calculated and an experimental diffraction pattern. For more detailed information on this topic, which is out of the aim of this review, see Refs. 13-15. An updated review on the advances in total scattering analysis can be also found in ref 18. After this brief introduction to the PDF technique, we will present recent examples of the application of PDF analysis to functional materials.

3. PDF studies of functional materials

3.1 Oxide ion conductors

Acceptor doped ZrO_2 was the first oxide ion conductor investigated by means of X-ray PDF by by Gateshki *et al.* in 2005¹⁶ with the aim of correlating the average and local structure of nanocrystalline samples. More recently, doped CeO_2 , was the subject of total scattering investigation. Doped CeO_2 ($Ce_{1-x}RE_xO_{2-x/2}$) is a fluorite type conductor which is typically doped with Rare Earth elements, with the best electrochemical performances obtained with ions which minimize the size difference with respect to Ce^{4+} (Sm, Gd and Y). However, doping levels above x ca. 0.20 usually lead to a dramatic reduction of the ionic conductivity. Different explanations for this behaviour were proposed. Among these, the most commonly accepted are the possible formation of complex defects, the oxygen vacancies ordering or the phase separation at the

nanoscale. Great efforts were made in order to elucidate such behaviour at the microscopic level and doped ceria has been extensively studied by means of several different experimental and computational techniques such as EXAFS, HRTEM, X-ray and neutron diffraction and atomistic modelling. In spite of this, the possible presence of extended defect clusters as well as their nature and dimensions as function of the dopants were far from being clarified. In this context, a relevant PDF study was carried out in 2012 by Scavini *et al.*¹⁷ in order to investigate the nature and the correlation length of defects clustering in the $Ce_{1-x}Gd_xO_{2-x/2}$ solid solution. Experimental pair distribution functions of samples with different compositions were fitted starting from their average crystallographic structure, *i.e.* the fluorite type structure for samples with $x < 0.50$ and the C-type structure for samples with $x > 0.50$. Good fit agreement between experimental data and model structures was obtained, for all the samples, only for $r > 10$ Å; for r values shorter than 10 Å a clear worsening of the fits quality was evident, as can be seen in Figure 2¹⁷. The introduction, in the structural model, of defect clusters following the indication coming from molecular dynamic simulations did not lead to any improvement of the fit quality. A significant improvement in the description of the experimental PDFs was obtained by a two-phase refinement with both CeO_2 and Gd_2O_3 structures (see Figure 3¹⁷).

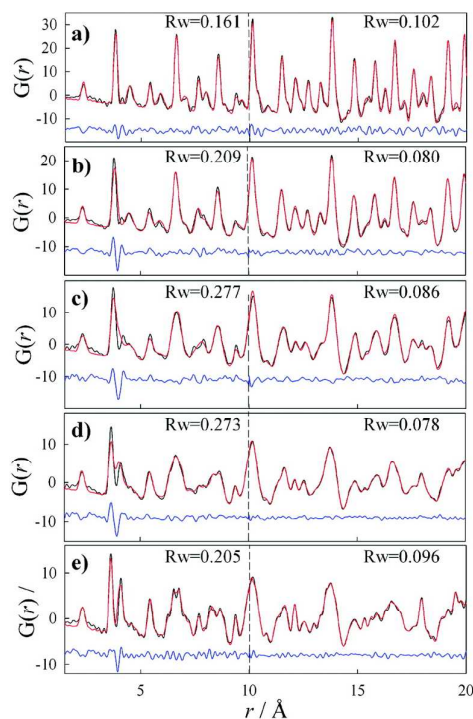
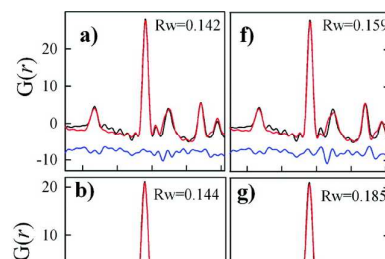


Figure 2: (a-e) $G(r)$ refinements using the real space Rietveld method over different r ranges for $x_{Gd} = 0.125, 0.25, 0.50, 0.75, 0.875$ samples respectively. Experimental (black), calculated (red) and residual profiles (blue) are shown. Reprinted with permission from M. Scavini *et al.*, *Chem. Mater.*, 2012, **24**, 1338-1345. Copyright 2012 American Chemical Society.



from 1173 to 1313 K, and cubic above 1313 K. It becomes a suitable oxide ion conductor slightly above 1200 K when the oxygen vacancies start to disorder and the oxygen migration is favoured. For this reason many doping strategies have been proposed in literature in order to stabilize the tetragonal and cubic structures of barium indate, among which one of the most interesting is the oxyanionic doping with PO_4^{3-} and SO_4^{2-} ions²¹. Moreover, computational studies reported a distribution of the oxygen vacancies for this system far from being random even at highest temperatures suggesting some discrepancy between the short range order and the average crystallographic structure²². In this context, an X-ray total scattering investigation at room temperature of the orthorhombic pure barium indate and the doped samples $\text{Ba}_2\text{In}_{1.70}\text{P}_{0.30}\text{O}_{5.30}$ and $\text{Ba}_2\text{In}_{1.70}\text{S}_{0.30}\text{O}_{5.45}$ (which are cubic at room temperature), was carried out with the aim of looking at their local structure and testing the available theoretical models which suggested a similar local order for the different average structures. The results of this work indicated that the two doped samples, which clearly show a cubic symmetry in the medium to long range, in agreement with X-ray and neutron diffraction patterns, show, on the other hand, a distorted orthorhombic symmetry at the local scale. This can be seen for the sulphate ion doping from the fits reported in Figure 4²⁰. This more distorted atomic arrangement at local scale, once the defects become mobile, allow an easier mobility of the oxide ions and can be ascribed as the reason making the cubic phase more conductive than the orthorhombic one.

Non-conventional oxide ion conductors of recent discovery were also the object of intense total scattering investigations. Neutron PDF analysis was performed on a gallium melilite family compound, the $\text{La}_{1-x}\text{Sr}_x\text{Ga}_3\text{O}_{7+x/2}$ with $x = 0.50$ ²³. This compound was found to have a notable high purely ionic conductivity due to the interstitial oxygen, which is accommodated in the melilite structure in order to balance the La/Sr doping²⁴. The PDF study aimed at providing a deeper comprehension of the difectual structure of this oxide and in particular to give an experimental evidence of the actual localization of the interstitial oxygen in the melilite structure which is a basic requisite in order to understand the ion migration path.

The improvement resulted particularly evident for samples with a similar Ce and Gd content. All these findings, coupled to a detailed analysis of the bond distances maps of the CGO solid solution, lead the Authors to conclude that, in this system, Ce^{4+} and Gd^{3+} show the tendency to retain the local environment they have in the end members with coherence domains in the $r < 10 \text{ \AA}$ range thus indicating in this way the presence of extended defects at the local scale in the system. Similar results were also obtained by the same Authors for the $\text{CeO}_2/\text{Y}_2\text{O}_3$ solid solution¹⁸, which shows a local structure substantially different from the average and mesoscopic structures. On the other hand, ceria doping with Pr and Tb was found to behave differently, in particular with the retention of the cerium oxide structure but with different oxidation states for the two dopants¹⁹.

Another appealing conventional oxide ion conductor structure investigated was the brownmillerite structure which is an anion vacancy ordered variant of the perovskite structure. In particular, the system investigated was doped $\text{Ba}_2\text{In}_2\text{O}_5$ ²⁰ with particular emphasis on the role of oxyanionic doping on the structure. Pure barium indate is orthorhombic (s.g. *Icmm*) up to 1173 K, tetragonal

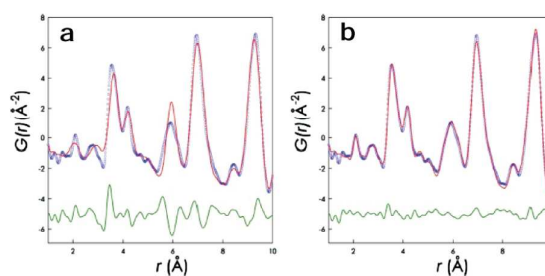


Figure 4: a) PDF fit of $\text{Ba}_2\text{In}_{1.70}\text{S}_{0.30}\text{O}_{5.45}$ up to 10 Å with the *Pm-3m* cubic space group and b) with the *Icmm* orthorhombic space group. Blue circles: experimental data; red line: calculated PDF; horizontal green line: residual. Reproduced from Ref. 20 with permission from The Royal Society of Chemistry.

Various structures, ranging from Rietveld derived models to computational models, were tested against the experimental data. The main results indicated that the interstitial oxygen lies in the

pentagonal ring cavity formed by the gallium coordination polyhedra and the best fit of the experimental neutron PDF was obtained for the structural model in which the defects are placed off-centred in such cavity. This result was recently confirmed by Xu *et al.*²³ by the comparison with Ce-substituted melilites.

A further development of the application of PDF analysis to challenging ion conductors is the coupling between experimental data and DFT analysis, which seems to be a required approach for systems where a description of the average structure of the anion sub-lattice becomes very complex. A recent example is the work by Kalland *et al.*²⁵ where a neutron and X-ray total scattering study has been coupled to extensive molecular dynamic simulation. In particular, object of such work was to shed light on the actual structure of the most recent discovered oxide ion conductor, the lanthanum tungstate, which was initially described in the literature with the chemical formula $\text{La}_6\text{WO}_{12}$, similarly to other rare earth tungstates. First studies found that the material can exist in a stable phase only for La/W atomic ratios between 5.3 and 5.7, and the structure was described as a complex fluorite type cubic structure (s.g. *F-43m*) in which both lanthanum and tungsten are cubically coordinated by oxygens²⁶. More detailed structural studies, carried out by means of high resolution X-ray diffraction, detected a significant distortion from the cubic symmetry and an octahedral coordination of the tungsten atoms²⁷.

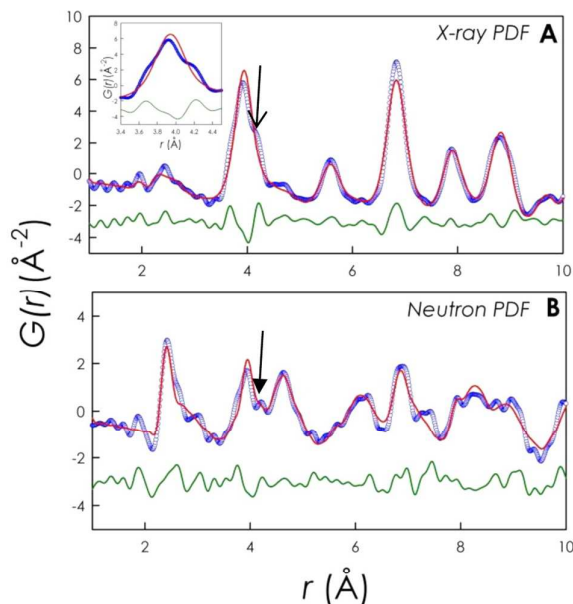


Figure 5: X-ray (Panel A) and neutron (Panel B) PDF refinements of lanthanum tungstate by means of the average tetragonal space group reported in ref 12; agreement factor for the fits are $R_{wp} = 0.188$ and 0.327 respectively. Inset of Panel A: detailed view of a selected region around the peak located at ~ 4 Å. Blue circles: experimental data; red line: calculated PDF; and horizontal green line: residual (shifted by -3 for ease of visualization). Reprinted with permission from L. E. Kalland *et al.*, *Chem. Mater.*, 2013, **25**, 2378-2384. Copyright 2013 American Chemical Society.

As a consequence, the structure was refined with a tetragonal unit cell (s.g. *I4/mmm*) that reduced the maximum number of available oxygen sites from 64 to 56. In spite of all these experimental efforts,

the lanthanum tungstate structure still showed to be quite elusive, in particular concerning the oxygen ions distribution. Neutron and X-rays total scattering experiments were carried out and initially compared to the (average) structural models available in literature leading to the evidence of a significant grade of disorder in the oxygen sublattice, which is also evident from the marked background modulation in the neutron diffraction patterns. In addition, the fit of the experimental PDFs in the short range lead to unsatisfactory results, as can be seen in Figure 5²⁵, showing a strong discrepancy between the average crystallographic structure and the local range order. Following these results, and the extremely complex oxygen distribution, several different structural configurations of varying total energy obtained by molecular dynamic simulations, were fitted against the experimental X-ray and neutron PDFs. The interplay between molecular dynamics simulation results and PDF fitting allowed to identify the most plausible oxygen distribution as demonstrated by both X-ray and neutron PDF fitting agreement reported in Figure 6²⁵. The use of DFT calculations in order to derive energetically stable structural starting models has led to a good description of the experimental PDFs of this complex oxide. The combination of DFT and PDF can provide a very powerful method to understand structural details that cannot be simply accessed or verified. The coupling of PDF analysis with computational modelling represents an approach which is expected to play a central role in the structural characterization of new advanced functional materials in the next future.

3.2 Li-ion battery materials

Lithium-ion batteries (LIBs) have become, in the past decade, the most important rechargeable energy storage devices and nowadays they are used for a bunch of different mobile equipment as power tools like cellphones and laptops, and they are also promising candidates for automotive applications. Although in these years their performance have impressively improved, many materials science issues still remain to be solved for a wider diffusion and cost reduction of this technology. Several total scattering works, dealing with both anode and cathode materials, have recently appeared in literature. The reason for the popularity of PDF analysis in the LIBs field can be explained by considering the following aspects: *i*) the common presence of components that have poor crystallinity (or that are amorphous); *ii*) the marked presence of static and/or dynamic disorder; and *iii*) the fact that the processes and the reactions occurring are often affected by nano- and meso-scale effects and domains. Positive electrode (or cathodic) materials have been extensively studied essentially in order to improve their energy density. Layered oxides, polyanionic compounds and 3D transition metal binary compounds represent a sort of timeline of the materials discovery in this research field which couples with the increase in the complexity of the systems and the electrochemical processes involved. Total scattering studies were carried out for all these classes of materials in order to unveil new structural details of relevance for the applications of LIBs.

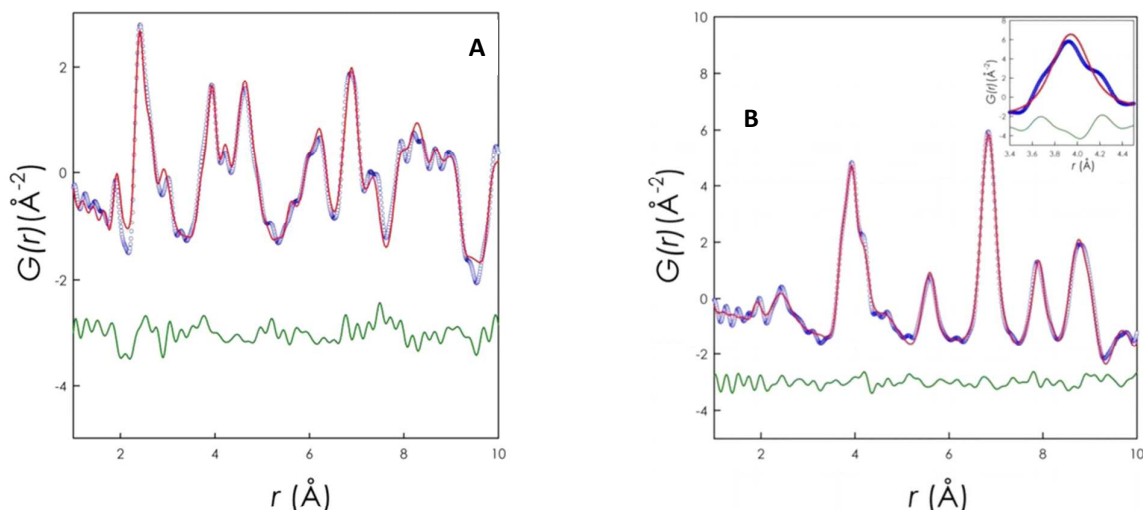


Figure 6: Neutron (panel A) and X-ray (panel B) PDF refinements by means of DFT calculated local structure for the lanthanum tungstate; agreement factor values are Rwp = 0.168 and 0.098 respectively. Blue circles: experimental data; red line: calculated PDF; and horizontal green line: residual (shifted by -3 for ease of visualization). Adapted with permission from L. E. Kalland *et al.*, *Chem. Mater.*, 2013, **25**, 2378-2384. Copyright 2013 American Chemical Society.

Among others, relevant examples are Idemoto *et al.*²⁸ where the correlation between the synthesis and the local structure of the $x\text{Li}(\text{Li}_{1/3}\text{Mn}_{2/3})\text{O}_2-(1-x)\text{Li}(\text{Mn}_{1/3}\text{Ni}_{1/3}\text{Co}_{1/3})\text{O}_2$ solid solution is reported; Adipranoto *et al.*²⁹ where the crystal and local effects of the Ni doping in $\text{LiCo}_{1-x}\text{Ni}_x\text{O}_2$ system is carefully examined, leading to the conclusion that the distance of diffusion pathways of oxide ions around Co atoms does not change when it is substituted with Ni; Moriya and coworkers³⁰ which reported a study of the charged/discharged structures of carbon hybridized $\text{Li}_2\text{MnSiO}_4$ nanoparticles in which is evident the repetitive disappearance/appearance of the long range order of the lithium manganese orthosilicate during the charge/discharge processes, respectively, with the consumption of the long range order due to distortions of the $[\text{MnO}_4]$ octahedra; and the neutron PDF investigation of the rich polymorphism showed by the Li_2MSiO_4 family (with $M = \text{Fe}, \text{Mn}$), reported in ref. 31, showing that all the polymorphs investigated have the same monoclinic distortion in the short range, thus suggesting a possible explanation for the similar electrochemical behavior of the different average crystallographic structures.

More articulated works have been made on transition metals binary compounds, in particular by coupling the PDF technique with *in situ* or *in operando* solid state NMR. A very elegant example of such powerful multi-combined investigation can be found in Wiaderek *et al.*³², where the Authors provided a very detailed description of the structural and electrochemical processes which take place in the mixed anion cathode FeOF during cycling. This work can be considered an evolution of the investigation reported in Yamakawa and coworkers³³ in 2009, where the same combination of total scattering analysis (in this case *ex situ* measurements) and solid state NMR is used to describe the conversion mechanism of the FeF_3 composite cathodic materials.

As previously outlined, PDF analysis plays a central role in this kind of studies because the general characterization challenge for conversion based cathodes comes from the alternate consumption/renovation of the long range order during charge-discharge cycles. In the work by Wiaderek *et al.*³², the PDF technique was strengthened by the coupling with solid state NMR technique, that provides further structural and chemical information on active species (*i.e.* lithium ions and fluorine). However the coupled PDF-NMR approach can be extremely powerful by performing *in situ* measurements. It is worth to point out that this work represents, in particular, the first example of such kind of *in situ* PDF measurement.

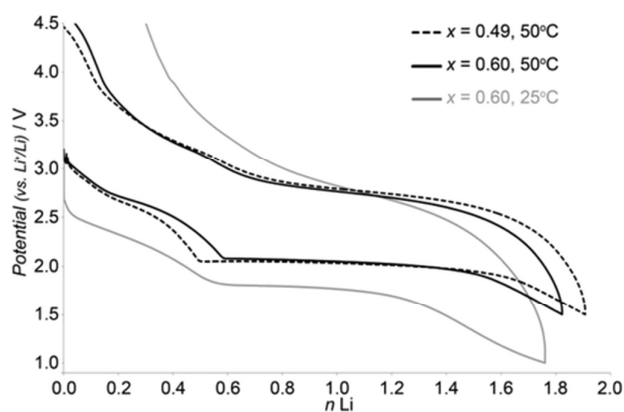


Figure 7: Discharge-charge curves obtained for $\text{Fe}^{\text{II}(1-x)}\text{Fe}^{\text{III}}_x\text{O}_2\text{F}_{2-x}$ within the AMPIX cell presented in Ref. 32 during PDF measurements, with a cycling current of 30 mA/g. Reprinted with permission from K. M. Wiaderek *et al.*, *J. Am. Chem. Soc.*, 2013, **135**, 4070-4078. Copyright 2013 American Chemical Society.

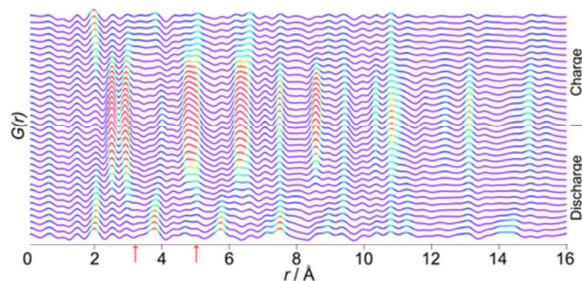


Figure 8: Selected PDFs obtained during the first discharge-charge cycle (for $x = 0.60$, $50\text{ }^{\circ}\text{C}$, $C/30$, $\sim 35\text{ h}$, $4.5\text{--}1.5\text{--}4.5\text{ V}$). The arrows indicate distances characteristic of the rock salt intermediate. The colors reflect relative peak intensities. Reprinted with permission from K. M. Wiaderek *et al.*, *J. Am. Chem. Soc.*, 2013, **135**, 4070-4078. Copyright 2013 American Chemical Society.

From an experimental point of view, the Authors measured several *in situ* PDFs during electrochemical discharge-charge cycles whose curves are reported in Figure 7³²; in parallel, Figure 8³², shows selected PDFs obtained during the first cycle. Similar features and trends can be appreciated and the structural transitions observed during charge and discharge result largely reversible. The discharge product was identified as metallic Fe nanoparticles, which is characterized by the short Fe-Fe correlations at 2.5 \AA . An additional intermediate phase, observed both during charge and discharge processes, is identified by peaks at 3.2 and 5.0 \AA which are absent in the charged (pristine) or discharged states. The product at the end of the charge shows atomic correlations below 5 \AA , similarly to the pristine starting structure of the electrode, although the peaks at longer distances result attenuated, suggesting a reduction in crystallinity or in the particle size. Experimental PDFs were fitted with structural models in order to identify the evolution of the phases in the system and their particle sizes. The analysis reports a progressive disorder in the pristine phase during the initial discharge with the formation of several crystalline, distorted and amorphous rutile-type $\text{FeO}_x\text{F}_{2-x}$ phases with no evidence of local O/F ordering. In addition, the intermediate outlined above (which starts to form after about 0.4Li , *i.e.* just before the plateau in the electrochemistry reported in Figure 7³²) was identified as a not stoichiometric rock salt type $\alpha\text{-LiFeO}_2$ phase, with coherent particles size of 50 \AA . During discharge, Fe nanoparticles are formed with particle size of about 25 \AA . Upon charge, these nanoparticles are consumed, forming a poorly ordered, or “amorphous”, rutile phase which shows partially ordered features only below $6\text{--}10\text{ \AA}$. Finally, rock salt phase does not react until all the Fe nanoparticles have been completely transformed in “amorphous” rutile. Authors provide also bond valence sum analysis where the weighting of Fe-O to Fe-F bond valence parameters provides a measure of the ratio between Fe-F and Fe-O bonds throughout the entire process. For example, it was clearly shown that Fe-F bonds decreases linearly between 0.6Li and 1.4Li with exclusively Fe-O remaining in the oxidized Fe phase at the end of the discharge; this suggested that rock salt phase is primarily an oxide. Parallel to this, during discharge, also F-coordinated Fe was clearly shown to be

preferentially reduced to Fe nanoparticles and LiF. Thanks to the data collected, the Authors could give a very detailed and precise description of the full discharge-charge process at the microscopic level. Moreover, an important further conclusion is that the active cathode, which delivers the enhanced performance, is actually a two phase composite mixture of oxide-rich and fluorine-rich materials instead of a single oxyfluoride phase. This suggests that synthesis efforts made in order to obtain the single phase mixed-anion compound are unnecessary and that similar enhanced performances in conversion systems could be obtained using composite cathodes which simply are physical mixtures of oxides and fluorides.

A similar investigation on the carbon coated CuF_2 conversion cathode, was reported by Hua *et al.*³⁴. As in ref. 32, here the Authors carried out an *in situ* PDF analysis coupled with solid state NMR in order to elucidate the entire lithiation mechanism over a full cycle. All the experimental evidences collected lead authors to a number of interesting conclusions not reported before: *i)* CuF_2 is found to participate only to the first discharge while very little or no copper fluoride formation is detected upon charge; *ii)* the amount of small Cu nanoparticles formed on discharge grows at the beginning of the CuF_2 conversion enhancing the electronic conductivity and helping to compensate for insulating effects due to the LiF phase; *iii)* formed Cu nanoparticles are largely covered by an insulating LiF layer, helping to prevent their sintering; *iv)* SEI formation on the Cu surfaces enlarges the overpotential causing a continuous potential reduction; *v)* the CuF_2 conversion mechanism is essentially different from most of the other conversion materials: due to the close potential for the Cu dissolution in the organic electrolyte to that for the reconversion reaction, Cu therefore dissolves in the electrolyte and consumes LiF thus preventing Cu to transform to CuF_2 . Finally, another combined experimental approach is presented in Wiaderek *et al.*³⁵, where PDF analysis is coupled to small angle X-ray scattering (SAXS) to study a series of different nano-composite cathodes of iron fluorides, oxyfluorides and oxides in order to probe the atomic and nanoscale structure in Fe formed through the electrochemical conversion in different anion environments.

Although less diffusely explored by means of PDF, also negative electroodic (anodic) materials were subject of total scattering investigations. First work of this kind on silicon anodes appeared in 2011 by Key and co-workers³⁶ reporting an *ex situ* PDF study in combination with solid state NMR technique. In particular, electrochemical phenomena at the anode during first discharge and subsequent charge cycles were modeled through a four-processes mechanism. Much work was made on the germanium based anodes, as for example in the paper by Liu *et al.*³⁷ where experimental PDFs from $\text{GeO}_2\text{-SnCoC}$ composite anode were collected and analyzed in order to describe the entire lithiation/delithiation process. PDF analysis was here particularly useful to reveal the reversible conversion reaction of GeO_2 and SnO_2 and to attribute this reversibility to the catalytic effect of a germanium-cobalt alloy formed during cycles. Also the simple germanium anode was tested and studied by means of the PDF technique and solid state NMR by Jung *et al.*³⁸. In this work the

Authors found that the lithiation process occurring in Ge anodes starts the formation of the Li_9Ge_4 phase instead of the previously reported Li_7Ge_3 ; the mechanism continues with the Li_7Ge_3 conversion to Li_7Ge_2 through several disordered phases containing columns of Li and Ge, and finally it ends with the nucleation and the growth of the crystalline $\text{Li}_{15}\text{Ge}_4$ phase, which can be further lithiated to $\text{Li}_{15+6}\text{Ge}_4$.

We would like to highlight that most of the results presented in this section were possible thanks to PDFs measurements carried out at the 11-ID-C and 11-ID-B beamlines at the Advanced Photon Source synchrotron, which greatly contributed in the last years to the evolution of the X-Ray total scattering technique in order to afford the most challenging and actual problems in material science.

3.3 Hydrogen storage materials

Application of total scattering methods to the hydrogen storage materials field show how the PDF analysis could be fundamental in order to understand mechanistic properties and processes.

For example, in Kim *et al.*³⁹ the structural changes of the $\text{V}_{1-x}\text{Ti}_x$ alloy were investigated in the early hydrogen absorption and desorption cycles. Vanadium is a very suitable material for hydrogen storage but its high cost represents one important drawback for real applications. However, it is well known that alloying V with inexpensive elements such as, for example, Ti, usually leads to a significant reduction in hydrogen storage properties due to the possible increase of defects and lattice strains. Although this general awareness, the mechanism behind the degradation in the reversible hydrogen storage capacity in vanadium based alloys during hydrogen cycling was not fully elucidated. Authors of ref [39] observed an unusually rapid profile damping in the collected experimental PDFs during first hydrogen absorption and desorption cycles for pure vanadium sample with such phenomenon becoming faster by increasing the Ti concentration in the alloy. Absence of any extra peak appearing in the low r -range region during cycles ruled out the possibility of secondary phases formation as the reason for the degradation in reversible hydrogen uptake.

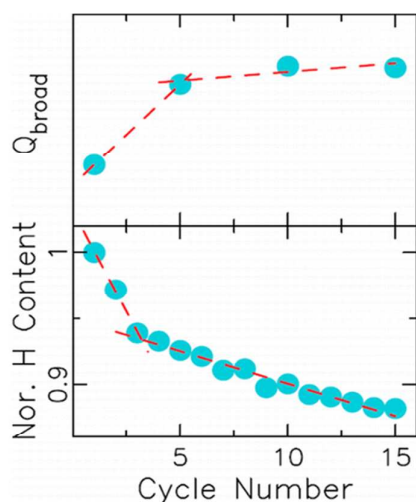


Figure 9: (a) Q_{broad} values obtained from the PDF refinements of $\text{V}_{0.9}\text{Ti}_{0.1}\text{H}_2$ data and (b) the reversible hydrogen storage capacity of $\text{V}_{0.8}\text{Ti}_{0.2}$ at 413 K are plotted as a function of cycle number. The reversible hydrogen storage capacity was normalized by the initial value. Red dashed lines are for guidance. Reprinted with permission from H. Kim *et al.*, *J. Phys. Chem. C*, 2013, **117**, 26543-26550. Copyright 2013 American Chemical Society.

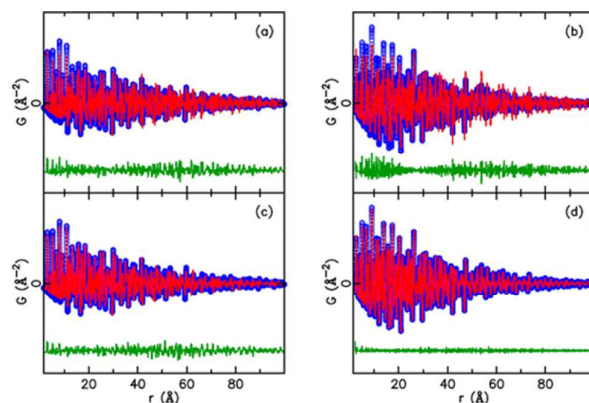


Figure 10: Calculated PDFs using (a) the VH_2 stacking fault model and (b) V dislocation model were fitted using the defect-free models without refining the Q_{broad} parameter. Blue open circles, red lines, and green lines represent calculated PDFs using the defect models, fits using the defect-free models, and difference curves, respectively. The difference curves are offset for sake of clarity. (c) and (d) refinement of the same PDFs as (a) and (b) with Q_{broad} parameter, respectively. Q_{broad} parameter did not help explain the effect of stacking faults (c) but reproduced the effect of dislocations on the PDF very well (d). Reprinted with permission from H. Kim *et al.*, *J. Phys. Chem. C*, 2013, **117**, 26543-26550. Copyright 2013 American Chemical Society.

The broadening of PDF peaks during absorption/desorption cycles can be appreciated in Figure 9³⁹ in the increasing Q_{damp} values versus the number of cycles. This continuous broadening and the fast functions damping was therefore correlated to lattice defects or disorder which could disturb mid to long range structural order and play an evident role in the worsening of the storage performance of the $\text{V}_{1-x}\text{Ti}_x$ alloy. As a consequence, various defects between stacking faults, twin boundaries, dislocations and vacancies were tested with the help of MD simulations in order to understand the origin of this effect. Fits with a structural model containing dislocations gave so far the best results as reported in Figure 10³⁹ indicating that the increase in the concentration of such defects is the reason for the reduction in the reversible hydrogen storage capacity of vanadium-titanium alloy system. A similar approach was then adopted by the same research group in Sakaki *et al.*⁴⁰ to solve the structure-properties correlation problem for a different material for hydrogen storage, *i.e.* the $\text{Mg}_{2-x}\text{Pr}_x\text{Ni}_4$ system. Also in this case, it was found that the reduction of hydrogen storage capacity is caused by the accumulation of dislocations introduced during hydrogenation in the early stages of the cycling process. Both the works presented in this paragraph were possible thanks to the high quality total scattering data obtained on the BL22XU beamline at the Spring-8 synchrotron.

3.4 Porous materials

Several classes of materials characterized by high and diffuse porosity, which have attracted great interest in recent times, have been the object of relevant PDF studies. Among them, huge interest is nowadays devoted to metal organic frameworks (MOFs), consisting of metal ions networks linked in a three dimensional framework by organic electron-rich ligands. MOFs are characterized by an impressive chemical and structural versatility due to the wide range of possible components and substituents, and for this reason they also show a wide range of potential applications ranging from gas sorption and separation to catalysis, proton conduction and photoluminescence. In particular, the interaction between the flexible MOFs structures with guest molecules represent an ideal field of investigation for the PDF analysis.

Exemplary studies can be found in Sava *et al.*^[41] and Chapman *et al.*^[42], where the capture of the volatile iodine fission product by zeolitic imidazolate framework-8 is diffusely discussed. In these papers, the total scattering technique has a fundamental role in the comprehension of the host-guest interactions through the analysis of the difference between the PDFs of the unloaded and loaded samples. The same study was extended two years later in another paper by Sava *et al.*⁴³ where the subject of the investigation is the Cu-BTC metal organic frameworks, also known as HKUST-1, an hydrophilic open pores MOF containing coordinatively unsaturated metal centers. In this work the differential PDFs approach is adopted in order to isolate the correlations involving the sorbed species, *i.e.* the host-guest correlations. Furthermore, the intensity of the PDF peaks is correlated to the relative abundance of a given atom-atom pair: thus the intensity of the peaks due to Cu-O and I-I bonds (at about 2 and 2.7 Å, respectively) provides an estimation of the Cu/I ratio which is monitored during the room temperature isotherm for iodine sorption, as reported in Figure 11⁴³.

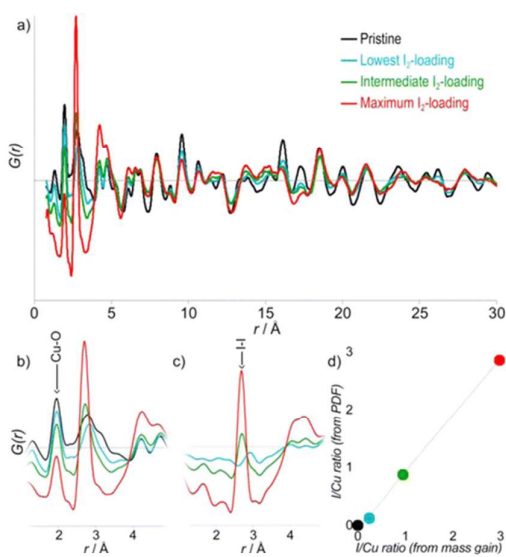


Figure 11: (a) The local and intermediate range structural information in the pair distribution functions (PDFs) confirms that the crystalline Cu-BTC lattice is retained at all I_2 loadings. The intensity of the peaks associated with the Cu-O and I-I correlations in the low- r regions of the (b) PDFs and (c) differential-PDFs, respectively, provide an estimate of the (d) I/Cu ratio, which matches that determined gravimetrically. Reprinted (adapted) with permission from D. F. Sava *et al.*, *Chem. Mater.* 2019, 31, 2991-2998. Copyright 2019 American Chemical Society.

Total scattering approach was recently applied also to a new sub-family of metal organic frameworks which show non-crystalline structures and for this reason are termed as amorphous MOFs (α MOFs)⁴⁴⁻⁴⁷. The absence of Bragg diffraction peaks in these materials precludes the determination of the atomic positions and of the long range structure. In spite of this, the disordered nature of α MOFs generates diffuse scattering, which contains important information on the atom-atom interactions and can be used to describe the short range order of these frameworks. Indeed, PDF analysis represents, by far, the fundamental tool to characterize the structure of these amorphous systems. Usually, Reverse Monte Carlo (RMC) modeling on PDF data can be used to obtain structural models which can be refined against experimental data in order to obtain characteristic structural parameters. Readers are referred to Ref. 48 in which an exhaustive summary of the PDF characterization on the α MOFs systems can be found. Nevertheless we would like to point out that, essentially, all the work made on such class of MOFs was possible thanks to the collection of neutron pair distribution function on the GEM diffractometer at ISIS at the Rutherford-Appleton Laboratories, which can be easily considered one of the most experienced instrument for the characterization of amorphous materials.

Mesoporous silica-based systems are another class of materials that have been recently studied with the help of the total scattering approach and that will be presented briefly in following. As in the case of the metal organic frameworks, the interaction between host species and guest structure provides the substrate on which PDF analysis can show all its power as a tool to derive structure-properties correlations. In 2013 Hsieh and coworkers reported a study⁴⁹ where a detailed description of the structural organization of a mononitrosyl complex host in a mesoporous silica matrix is given using a multiscale approach and combining PDF analysis with solid state NMR. One year later, the same group published a new study⁵⁰ on porous silica that incorporates crystalline nanoparticles of sodium nitroprusside with average diameter of 6 nm filling almost completely the matrix pores in order to shed light on the stability of the host species as function of the external parameters. All of these works demonstrate the increasing interest in using PDF analysis to characterize host-guest interactions inside solid networks. Due to the feasibility and the effectiveness of the total scattering approach in solving this kind of structural problems, it is not utopian to foresee in the future a standardization of the PDF analysis as a structural probe for various categories of porous materials, also at an industrial level.

3.5 Materials for Catalysis

Nanomaterials for catalyst are among the most interesting and studied systems in materials science due to their extraordinary

versatility, high performances and wide range of possible applicative areas. Such characteristics come from the significant difference in the structural properties with respect to the corresponding bulk materials. In addition, most of these nanomaterials for catalyst are characterized by nanoscale structural features such as nano-domains and/or local segregation or high distortions at the surfaces, which cannot be easily detected and described with traditional crystallographic analysis. Pair distribution function can overcome these limitations and provide very useful insights through both the simple analysis of the distances distribution in the experimental functions and/or with model based analysis. Both approaches can easily discriminate between different atomic environments and take into account the local structural properties that determine the key aspects in the definition of the functional properties in such nanomaterials. For these reasons, PDF analysis have been extensively used to characterize this kind of systems and several works have been reported in the current literature with detailed structural characterization and processes descriptions. For example, a number of papers deal with the structural characterization of nanoalloys for catalytic purposes. In Loukrakpam *et al.*⁵¹ an interesting study on binary and ternary Pt-nanoalloys for the oxygen reduction reaction catalysis is reported. Authors of this paper determined the atomic scale structures of different nanoalloy catalysts and correlated different atomic ordering to differences in the electrocatalytic activities. In particular, ternary nanoalloy PtIrCo was found to have higher electrocatalytic activity in comparison with the binary counterparts and this behaviour was correlated with an increased shrunk metal-metal bonds distribution as can be seen in Figure 12⁵¹.

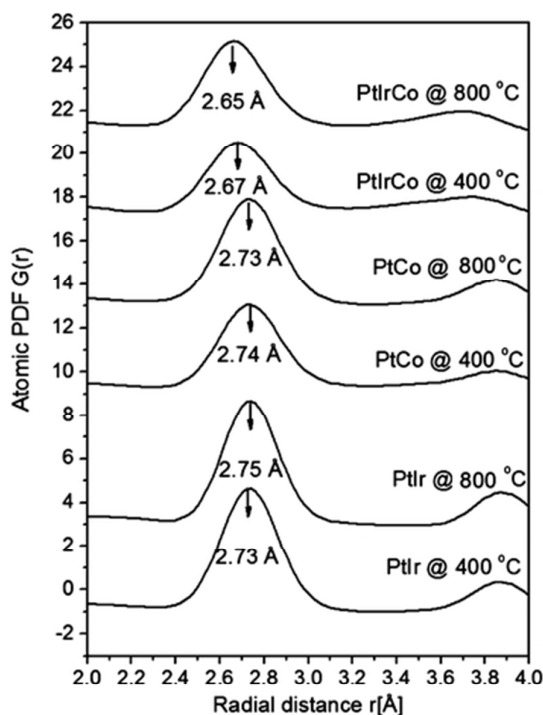


Figure 12: First peaks in the experimental atomic PDFs for different Pt-nanoalloys thermally treated at 400 and 800 °C. Positions of the peaks are estimated by Gaussian fits to the experimental data and are marked with arrows. Shorter distances were found for ternary alloy. Reprinted (adapted) with permission from R. Loukrakpam *et al.*, *J. Phys. Chem. C*, 2013, 117, 20719–20721. Copyright 2012 American Chemical Society.

Other works on Pt nanoparticles and monolayers/sub-monolayers supported on Au nanoparticles are reported in Refs. 52 and 53. Ref. 52 is a combined *in situ* PDF and XAS study which found interesting structural changes, *i.e.* contraction and relaxation, in 1-3 nm Pt nanoparticles induced by adsorption/desorption processes. Ref. 53 reports complete dehydrogenation of ethanol induced by Au nanoparticles on Pt monolayers and sub-monolayers with better electrocatalytic activity for the former one: in this work the PDF analysis was essential in order to reveal the 3D atomic ordering of the Au nanoparticles on the Pt layers. Pd-Ni nanoalloys were investigated by Shan and coworkers⁵⁴ in order to understand how exactly Pd and Ni atoms cooperate for the effective activation of CO species on the surface. In Petkov *et al.*⁵⁵ atomic ordering of nanosized metals and binary alloys of eleventh group elements was resolved by the coupling PDF analysis with reverse Monte Carlo modeling. Further, Petkov and co-workers⁵⁶ reported different catalytic activities for TiO₂ and SiO₂ supported gold nanoparticles which can be ascribed to different atomic scale structure of the nanoparticles.

3.6 Other Functional Materials

Several other interesting functional materials and phenomena have been recently investigated with success by means of the PDF analysis which are concisely reviewed in this section for sake of brevity. Nevertheless, we would include them in this review in order to give the idea of the wide range of present applications of the PDF analysis and future developments.

Hybrid perovskites are among those materials that attracted great interest in recent times for their performances and possible application as active materials in solar cells. In Choi *et al.*⁵⁷ X-ray PDF analysis was carried out in order to describe the structural behaviour of the methylammonium lead iodide (MAPbI₃) within a mesoporous TiO₂ layer, performing a quantitative modeling process. Approximately 70% of the active material was found in a highly disordered phase, important for the device efficiency, with local perovskite structure extending over a range of only 14 Å, which cannot be detected by conventional XRD measurements.

Negative thermal expansion (NTE) and zero thermal expansion (ZTE) materials have been fully characterized in typical systems thanks to the total scattering approach. For example, Bridges and co-workers⁵⁸ reported a combined PDF and EXAFS experiment on the ZrW₂O₈ compound, which is one archetype NTE material, finding correlated translational-rotational motions in the polyhedra network much more complicated than simple rotations that are previously used to account for its negative thermal expansion. In Hu *et al.*⁵⁹ an isotropic ZTE is reported over a wide temperature range in the ScF₃ system using chemical substitution on scandium site: this causes local rhombohedral distortion in the cubic average structure

which is the reason of the ZTE, and the distortion is evident looking at the differences in the short range of r -distances of the PDFs of pure and doped compounds.

Local structure and piezoelectric instability are correlated in BaTiO₃ system by Maurya and co-workers⁶⁰, where the role of A and B site substitution towards local structural changes and its correlation with the piezoelectric response were studied combining PDF analysis and Raman spectroscopy. The same approach, *i.e.* the combination with Raman spectroscopy, have been used on the same system also in Buscaglia *et al.*⁶¹, where an extensive description of the atomic ordering of the BaTi_{1-x}Zr_xO₃ series (with $x = 0.1, 0.2$ and 0.4) is given.

Pressure induced amorphization (PIA) is an interesting phenomenon which can be nicely investigated by means of total scattering methods. Examples can be found in Wilkinson *et al.*⁶² and Lu *et al.*⁶³ dealing with ZrMo₂O₈ and Ta₂O₅ nanowires, respectively. Notably, these papers witness both the evolution of the sample environments available for PDF experiments and the great engineering and scientific work done in order to overcome all the problems strictly correlated to the narrow angular window due to the utilization of pressure cells.

Another pretty rare and extremely interesting phenomenon recently addressed by means of PDF analysis is the emphanis, *i.e.* the appearance of a low symmetry state from a high symmetry state on warming due to a well-defined displacements of atoms from their centrosymmetric positions. In Knox *et al.*⁶⁴ the Authors provide a detailed X-ray and neutron PDF study of the SnTe structural changes as a function of temperature, pointing out a crossover to an emphanitic phase above 300 K with a relatively wide temperature range of about 100 K. Moreover, the emphanitic behaviour was found not to be related to the ferroelectric state of this compound, as previously suggested in the literature, but to a completely distinct phenomenon.

Application of the PDF analysis has also been proposed in order to solve some relevant pharmaceutical problems, such as the identification and quantification of phase fractions in mixed phase samples containing amorphous, nanocrystalline and crystalline components. Davis and co-workers⁶⁵ demonstrated the efficiency of the total scattering approach for this kind of applicative problems on the sulfamerazine antibiotic drug, describing significant different phase compositions for different samples preparation conditions, opening in this way the route to a new application which could find important industrial implications.

Finally we want to conclude this review by citing the brand-new combined computed tomography (TC) – PDF approach reported in Jacques *et al.*⁶⁶ for an Al₂O₃ catalytic system. Authors of this work push a step further on the way to the identification and characterization of materials which are lacking in long-range order. Combining computed tomography with PDF analysis under *operando* conditions gives the possibility to solve, both as a function of time and space, a working system which eventually can contain even amorphous or highly disordered phases, which is often the case of real material systems for catalysis or clean energy application like batteries and fuel cells. The spatial resolution can lead to unprecedented insight on reaction pathways, unequal

reaction kinetics in different parts of the systems and influence of the SEI formation. Furthermore the tomography can provide unique information, for example, on the response during working operation: of particular interest is the possibility to image the continuous mechanical degradation of the active materials or composites due to volume expansion or poisoning, which can cause a range of detrimental phenomena from mechanical cracking and deformation to irreversible deactivations. All the features arising from computed tomography are expected to further potentiate the total scattering analysis in order to fully describe and understand intercalation/deintercalation mechanisms, migration and catalytic processes. As for the previous case, also relevant industrial application could be imagined and considered in order to highlight once more the importance of such combined approach of structural characterization.

4. Conclusions

In this Feature Article we reported a number of recent works concerning the application of total scattering methods and pair distribution function analysis to materials chemistry problems with particular emphasis to functional materials. Growing number of related published research and dedicated instruments in international facilities all over the world demonstrate the growing interest of the materials science community in adopting total scattering approach as a core structural characterization tool. PDF analysis takes into account the structural deviations from the long range order thus being an ideal tool in order to unveil structural details otherwise not detectable with traditional crystallographic methods. For this reason the PDF analysis results particularly suitable in systems which are made of materials with a high degree of disorder, nanocrystalline compounds or amorphous phases, which may be the case of the new generation of advanced functional materials. Combination of total scattering approach with other solid state analysis techniques, such as solid state NMR, IR, and Raman spectroscopy, could significantly expand the range of the obtainable information. As discussed in this review, the synergy between PDF analysis and such other techniques has shown recently to be extremely useful in order to fully characterize and describe processes (and related mechanisms) of central relevance for modern materials chemistry such as Li intercalation/deintercalation or degradation in hydrogen storage systems. Brand-new experimental approaches and methodology just appeared in the field of total scattering, such as pharmaceutical-related works or the combination with computed tomography, already showed an enormous potential to solve still inaccessible structural-related problems.

To conclude, the increasing number of PDF-dedicated beamlines in synchrotrons around the world, together with the continuous development of user-friendly software by several groups⁶⁷⁻⁷⁵ and the interest showed by several companies in developing laboratory-scale PDF instruments, are going to make the PDF analysis the structural characterization technique of choice in modern materials science.

Acknowledgements

The Authors acknowledge the financial support for their research work provided by Cariplo Foundation (project 2013-0632) and the provision of beam time at ORNL, ESRF, and APS facilities.

Notes and references

‡ Footnotes relating to the main text should appear here. These might include comments relevant to but not central to the matter under discussion, limited experimental and spectral data, and crystallographic data.

§

§§

etc.

- C. A. Young, A. Goodwin, *J. Mater. Chem.*, 2011, **21**, 6464-6476.
- S. J. L. Billinge, *J. Solid State Chem.*, 2008, **181**, 1695-1700.
- L. Malavasi, *Dalton Trans.*, 2011, **40**, 3777.
- T. Egami, S. J. L. Billinge, *Underneath the Bragg peaks: structural analysis of complex materials*, Pergamon, Amsterdam; Boston, 2003.
- C. N. J. Wagner, *J. Non-Crystal. Solids*, 1978, **31**, 1.
- Y. Waseda, *The structure of non-crystalline materials*, McGraw-Hill, New York, 1980.
- I. K. Jeong, F. Mohiuddin-Jacobs, V. Petkov, S. J. L. Billinge and S. Kycia, *Phys. Rev. B*, 2001, **63**, 205202.
- S. Bruhne, E. Uhring, K.D. Luther, W. Assmus, M. Brnelli, A.S. Masadeh, S.J.L. Billinge, *Z. Kristallogr.*, 2005, **220**, 962.
- B.H. Toby, T. Egami, *Acta Crystallogr. A*, 1992, **48**, 336.
- I. K. Jeong, R. H. Heffner, M. J. Graf, S. J. L. Billinge, *Physical Review B*, 2003, **67**, 104301.
- C. L. Farrow, P. Juhas, J. W. Liu, D. Bryndin, E. S. Boin, J. Bloch, T. Proffen, S. J. L. Billinge, *Journal of Physics Condensed Matter*, 2007, **19**, 335219.
- T. Proffen, S. J. L. Billinge, *Journal of Applied Crystallography*, 1999, **32**, 572-575.
- D. A. Keen, M. G. Tucker, M. T. Dove, *Journal of Physics: Condensed Matter*, 2005, **17**, S15-22.
- D. A. Keen, A. L. Goodwin, M. G. Tucker, M. T. Dove, J. S. O. Evans, W. A. Crichton, M. Brunelli, *Physical Review Letters*, 2007, **98**.
- A. L. Goodwin, M. G. Tucker, M. T. Dove, D. A. Keen, *Physical Review Letters*, 2005, **95**, 119901.
- M. Gateshki, V. Petkov, G. Williams, S.K. Pradhan, Y. Ren, *Phys. Rev. B*, 2005, **71**, 224107.
- M. Scavini, M. Coduri, M. Allieta, M. Brunelli, C. Ferrero, *Chem. Mater.*, 2012, **24**, 1338-1345.
- M. Coduri, M. Scavini, M. Allieta, M. Brunelli, C. Ferrero, *Chem. Mater.*, 2013, **25**, 4278-4289.
- M. Coduri, M. Scavini, M. Brunelli, E. Pedrazzin, P. Masala, *Solid State Ionics*, 2014, **268**, 150-155.
- A. Mancini, J. F. Shin, A. Orera, P. R. Slater, C. Tealdi, Y. Ren, K. L. Page, L. Malavasi, *Dalton Trans.*, 2012, **41**, 50-53.
- J. F. Shin, A. Orera, D. C. Apperley, P. R. Slater, *J. Mater. Chem.*, 2011, **21**, 874.
- C. E. Mohn, N. L. Allan, C. L. Freeman, P. Ravindran, S. Stølen, *J. Solid State Chem.*, 2005, **178**, 346.
- A. Mancini, C. Tealdi, L. Malavasi, *Int. J. Of Hydrogen Storage*, 2012, **37**, 8073-8080; J. Xu, X. Kuang, E. Véron, M. Allix, M. R. Sucomel, F. Porcher, C. Liang, F. Pan, M. Wu, *Inorg. Chem.*, 2014, **53**, 11589-11597.
- X. Kuang, M. A. Green, H. Niu, P. Zajdel, C. Dickinson, J. B. Claridge, L. Jantsky, M. J. Rosseinsky *Nat. Mater.*, 2008, **7**, 498.
- L. E. Kalland, A. Magrasò, A. Mancini, C. Tealdi, L. Malavasi, *Chem. Mater.*, 2013, **25**, 2378-2384.
- A. Magrasò, C. Frontera, D. Marrero-Lopez, P. Nunez, *Dalton Trans.*, 2009, **46**, 10273-10283.
- A. Magrasò, J. M. Polfus, C. Frontera, J. Canales-Vasquez, L. E. Kalland, C. H. Hervoches, S. Erdal, R. Hancke, M.S. Islam, T. Norby, R. Haugrud, *J. Mater. Chem.*, 2012, **22**, 1762-1764.
- Y. Idemoto, M. Inoue, N. Kitamura, *Journal of Power Sources*, 2014, **259**, 195-202.
- D. S. Adipranoto, T. Ishigaki, A. Hosikawa, K. Iwase, M. Yonemura, K. Mori, T. Kamiyama, Y. Morii, M. Hayashi, *Solid State Ionics*, 2014, **262**, 92-97.
- M. Moriya, M. Miyahara, M. Hokazono, H. Sasaki, A. Nemoto, S. Katayama, S. Hirano, Y. Ren, *Journal of Power Sources*, 2014, **263**, 7-12.
- A. Mancini, V. R. Barbieri, J. C. Neufeind, K. Page, L. Malavasi, *J. Mater. Chem. A*, 2014, **2**, 17867-17874.
- K. M. Wiaderek, O. J. Borkiewicz, E. Castillo-Martinez, R. Robert, N. Pereira, G. G. Amatucci, C. P. Grey, P. J. Chupas, K. W. Chapman, *J. Am. Chem. Soc.*, 2013, **135**, 4070-4078.
- N. Yamakawa, M. Jiang, B. Key, C. P. Grey, *J. Am. Chem. Soc.*, 2009, **131**, 10525-10536.
- X. Hua, R. Robert, L. S. Du, K. M. Wiaderek, M. Leskes, K. W. Chapman, P. J. Chupas, *J. Phys. Chem. C*, 2014, **118**, 15169-15184.
- K. M. Weiderek, O. J. Borkiewicz, N. Pereira, J. Ilavsky, G. G. Amatucci, P. J. Chupas, K. W. Chapman, *J. Am. Chem. Soc.*, 2014, **136**, 6211-6214.
- B. Key, M. Morcrette, J. M. Terascon, C. P. Grey, *J. Am. Chem. Soc.*, 2011, **133**, 503-512.
- B. Liu, A. Abouimrane, M. Balasubramanian, Y. Ren, K. Amine, *J. Phys. Chem. C*, 2014, **118**, 3960-3967.
- H. Jung, P. K. Allan, Y. Y. Hu, O. J. Borkiewicz, X. L. Wang, W. Q. Han, L. S. Du, C. J. Pickard, P. J. Chupas, K. W. Chapman, A. J. Morris, C. P. Grey, *Chem. Mater.*, 2015, **27**, 1031-1041.
- H. Kim, K. Sakaki, H. Ogawa, Y. Nakamura, J. Nakamura, E. Akiba, A. Machida, T. Watanuki, T. Proffen, *J. Phys. Chem. C*, 2013, **117**, 26543-26550.
- K. Sakaki, N. Terashita, H. Kim, E. H. Majzoub, A. Machida, T. watanuki, S. Tsunokake, Y. Nakamura, E. Akiba, *J. Phys. Chem. C*, 2014, **118**, 6697-6705.
- D. F. Sava, M. A. Rodriguez, K. W. Chapman, P. J. Chupas, J. A. Greathouse, P. S. Crozier, T. M. Nenoff, *J. Am. Chem. Soc.*, 2011, **133**, 12398.
- K. W. Chapman, D. F. Sava, G. J. Halder, P. J. Chupas, T. M. Nenoff, *J. Am. Chem. Soc.*, 2011, **133**, 18583.
- D. F. Sava, K. W. Chapman, M. A. Rodriguez, J. A. Greathouse, P. S. Crozier, H. Zhao, P. J. Chupas, T. M. Nenoff, *Chem. Mater.*, 2013, **25**, 2591-2596.
- T. D. Bennett, S. Cao, J. C. Tan, D. A. Keen, E. G. Bithell, P. J. Beldon, T. Friscic, A. K. Cheetham, *J. Am. Chem. Soc.*, 2011, **133**, 14546-14549.
- T. D. Bennett, D. A. Keen, J. C. Tan, E. R. Barney, A. L. Goodwin, A. K. Cheetham, *Angew. Chem. Int. Ed.*, 2011, **50**, 3067-3071.
- S. Cao, T. D. Bennett, D. A. Keen, A. L. Goodwin, A. K. Cheetham, *Chem. Commun.*, 2012, **48**, 7805-7807.
- E. O. R. Beake, M. T. Dove, A. E. Phillips, D. A. Keen, M. G. Tucker, A. L. Goodwin, T. D. Bennett, A. K. Cheetham, *J. Phys.: Condens. Matter*, 2013, **25**, 395403.
- T. D. Bennett, A. K. Cheetham, *Acc. Chem. Res.*, 2014, **47**, 1555-1562.
- K. Y. Hsieh, E. E. Bendeif, A. Gansmuller, S. Pillet, T. Woike, D. Schaniel, *RSC Adv.*, 2013, **3**, 26132-26141.
- E. E. Bendeif, A. Gansmuller, K. Y. Hsieh, S. Pillet, T. Woike, M. Zobel, R. B. Neder, M. Bouazaoui, D. Schaniel, *RSC Adv.*, 2015, **5**, 8895-8902.

- 51 R. Loukrakpam, S. Shan, V. Petkov, L. Yang, J. Luo, C. J. Zhong, *J. Phys. Chem. C*, 2013, **117**, 20715-20721.
- 52 Y. Lei, H. Zhao, R. D. Rivas, S. Lee, B. Liu, J. Lu, E. Stach, R. E. Winans, K. W. Chapman, J. p. Greeley, J. T. Miller, P. J. Chupas, J. W. Elam, *J. Am. Chem. Soc.*, 2014, **136**, 9320-9326.
- 53 R. Loukrakpam, Q. Yuan, V. Petkov, L. Gan, S. Rudi, R. Yang, Y. Huang, S. R. Brankovic, P. Srasser, *Phys. Chem. Chem. Phys.*, 2014, **16**, 18866-18876.
- 54 S. Shan, V. Petkov, L. Yang, J. Luo, P. Joseph, D. Mayzel, B. Prasai, L. Wang, M. Engelhard, C. Zhong, *J. Am. Chem. Soc.*, 2014, **136**, 7140-7151.
- 55 V. Petkov, S. Shastri, S. Shan, P. Joseph, J. Luo, C. J. Zhong, T. Nakamura, Y. Herbani, S. Sato, *J. Phys. Chem. C*, 2013, **117**, 22131-22141.
- 56 V. Petkov, Y. Ren, S. Shan, J. Luo, C. J. Zhong, *Nanoscale*, 2014, **6**, 532-538.
- 57 J. J. Choi, X. Yang, Z. M. Norman, S. J. L. Billinge, J. S. Owen, *Nano Lett.*, 2014, **14**, 127-133.
- 58 F. Bridges, T. Keiber, P. Juhas, S. J. L. Billinge, L. Sutton, J. Wilde, G. R. Kowach, *PRL*, 2014, **112**, 045505.
- 59 L. Hu, J. Chen, L. Fan, Y. Ren, Y. Rong, Z. Pan, J. Deng, R. Yu, X. Xing, *J. Am. Chem. Soc.*, 2014, **136**, 13566-13569.
- 60 D. Maurya, A. Kumar, V. Petkov, J. E. Mahaney, R. S. atiyar, S. Priya, *RSC Adv.*, 2014, **4**, 1283-1292.
- 61 V. Buscaglia, S. Tripathi, V. Petkov, M. Dappiaggi, M. Deluca, A. Gajovic, Y. Ren., *J. Phys.: Condens. Matter*, 2014, **26**, 055901.
- 62 A. P. Wilkinson, B. K. Greve, C. J. Ruschman, K. W. Chapman, P. J. Chupas, *J. Appl. Phys.*, 2012, **112**, 023511.
- 63 X. Lu, Q. Hu, W. Yang, L. Bai, H. Sheng, L. Wang, F. Huang, J. Wen, D. J. Miller, Y. Zhao, *J. Am. Chem. Soc.*, 2013, **135**, 13947-13953.
- 64 K. R. Knox, E. S. Bozin, C. D. Malliakas, M. G. Kanatzidis, S. J. L. Billinge, *Phys. Rev. B*, 2014, **89**, 01410.
- 65 T. Davis, M. Johnson, S. J. L. Billinge, *Cryst. Growth. Des.*, **2013**, **13**, 4239-4244.
- 66 S.D.M. Jacques, M. Di Michiel, S.A.J. Kimber, X. Yang, R.J. Cernik, A.M. Beale, S.J.L. Billinge, *Nature Communications*, **2013**, **4**, 2536.
- 67 C. L. Farrow, P. Juhas, J. W. Liu, D. Bryndin, E. S. Bozin, J. Bloch, T. Proffen and S. J. L. Billinge, *J. Phys.: Condens. Matter*, 2007, **19**, 335219.
- 68 X. Yang, P. Juhas, C. L. Farrow, S. J. L. Billinge, *ArXiv:1402.3163*. **V2**. 2014
- 69 L. Grandlund, S. J. L. Billinge, P. M. Duxbury, *Acta Cryst.*, 2015, **A71**, 392-409.
- 70 S. J. L. Billinge, C. L. Farrow, *J. Phys. Condens. Matter*, 2012, **25**, 45.
- 71 M. G. Tucker, D. A. Keen, M. T. Dove, A. L. Goodwin, Q. Hui, *J. Phys.: Condens. Matter*, 2007, **19**, 335218.
- 72 S. T. Norberg, M. G. Tucker, S. Hull, *J. Appl. Crystallogr.*, 2009, **42**, 179-184.
- 73 A. K. Soper, *Phys. Rev. B*, 2005, **72**, 104204.
- 74 T. Proffen, R. B. Neder, *J. Appl. Crystallogr.*, 1997, **30**, 171-175.
- 75 A. Simonov, T. Weber, W. Steurer, *J. Appl. Crystallogr.*, 2014, **47**, 1146-1152.